www.sensorsportal.com

Sensors & Transducers
Published by IFSA Publishing, S. L., 2024
http://www.sensorsportal.com

# Comparison of Experimental and Theoretical Modeling of Temperature Drift in Off-Diagonal GMI Sensors

* Pape Abdoulaye FAM, * Papa Silly TRAORE
and Mamaye Inès CORREA
Ecole Supérieure Polytechnique (ESP), Université Cheikh Anta Diop (UCAD), Dakar, Sénégal
Tel.: (+221) 77 399 99 41
E-mail: papasilly.traore@esp.sn

*Received: 11 June 2024 / Revised: 26 December 2024 / Accepted: 28 December 2024*
*Published: 30 December 2024*

**Abstract:** This article investigates the temperature sensitivity of digital Magneto-Impedance (GMI) sensors by comparing experimental data with theoretical predictions. The study demonstrates that the experimental results are in excellent agreement with the theoretical model, showing a high level of consistency within the examined dynamic range. Notably, the sensitivity of the sensor at the zero bias point is significantly lower than at other bias points, with a measured sensitivity of approximately -0.2 mΩ/°C, validating simulation predictions. The linearity around the zero bias point also aligns with theoretical expectations. The agreement between experimental and theoretical results is strong for positive fields and those near zero, with theoretical values within established confidence intervals. However, a significant discrepancy was noted between -10 and -31 µT, suggesting areas for further improvement. This work confirms the reliability of the theoretical model while identifying areas needing further research. It provides a basis for enhancing the thermal stability of GMI sensors and reducing temperature-induced drift, paving the way for advancements in magnetic sensing applications.

**Keywords:** GMI sensor, Temperature drift, Sensitivity, Off-diagonal configuration.

## 1. Introduction

The Giant Magneto-Impedance (GMI) effect observed in amorphous wires represents a significant advancement in the field of magnetic sensing technology [1]. This phenomenon occurs when a magnetic conductor, typically in the form of a wire with an amorphous structure, experiences a dramatic change in its electrical impedance under the influence of a high-frequency alternating current and an external magnetic field [2, 3]. The sensitivity of the GMI effect is such that even minor variations in the magnetic field can induce substantial changes in the impedance, making these materials highly attractive for applications that require precise magnetic field measurements [3].

GMI-based sensors are particularly noteworthy for their potential in creating highly sensitive magnetometers and magnetic sensors. These devices are capable of detecting extremely weak magnetic fields with high accuracy, which is crucial in a variety of domains. For instance, in biomedical imaging, GMI sensors can be used to detect tiny magnetic signals generated by biological tissues, providing valuable diagnostic information [4]. In geophysics, they can be employed to map subtle variations in the Earth's magnetic field, aiding in mineral exploration and environmental monitoring. Furthermore, their application in navigation systems and industrial automation highlights the versatility of GMI sensors in real-time magnetic field detection [4].

Despite these advantages, the broader adoption of GMI sensors has been hindered by a critical limitation:

their sensitivity to temperature fluctuations. The impedance of GMI materials is not only dependent on the magnetic field but also on the ambient temperature, which can cause significant drift in sensor readings [5]. This temperature-induced drift is particularly problematic in practical applications where the sensor may be exposed to varying environmental conditions. For example, in industrial settings or field applications, where temperatures can fluctuate widely, the accuracy of GMI sensors can be compromised, leading to unreliable data and reduced sensor performance.

To address these challenges, our study focuses on a detailed investigation of the temperature drift characteristics of GMI sensors. The aim is to quantify the impact of temperature variations on the impedance and performance of these sensors, and to explore potential methods for mitigating these effects. A rigorous experimental setup that allows us to measure the temperature dependence of the GMI effect is developed. This setup includes controlled thermal environments and measurement tools to ensure accurate data collection across a range of temperatures.

In addition to the experimental approach, we will compare our empirical results with theoretical models. These models, based on the underlying physics of the GMI effect, predict how temperature influences impedance changes in amorphous wires. By validating these models against experimental data, we aim to deepen our understanding of the temperature dependence of GMI sensors and identify strategies to improve their thermal stability.

Section 1 provides an understanding of the principle of the off-diagonal configuration of the GMI wire. Section 2 details a theoretical model of temperature sensitivity. Section 3 presents the measurement setup and compares the measurement results with the theoretical model. The paper concludes with a summary of findings and potential future directions.

## 2. The off-diagonal Configuration

After the discovery of GMI effect, micro-GMI wires were initially used in their classic configuration [2, 3]. This setup involves exciting the material by a current $i_1$, with the sensor output $v_1$, being the voltage measured across the element itself (Fig. 1.a). In the last two decades, a new GMI structure called, the off-diagonal configuration was discovered [6-8]. This new technique proposes measuring the field-modulated voltage $v_2$, across a pick-up coil coupled to the sensitive element, as illustrated in Fig. 1.b. Fig. 1 shows the structure of the classical and off diagonal configuration of the GMI wire.

This technique has long been used in Fluxgate sensors [9]. It is primarily based on the appearance of longitudinal magnetization within the wire when it is traversed by a high-frequency excitation current [6], which creates a circumferential field around the conductor. The axial component of this magnetization generates the flux that the pick-up coil can detect. One of the main advantages of this magnetic configuration is its potential to increase the sensor's sensitivity and to improves its linearity by improving the number of turns of the pick-up coil [7]. This new magnetic configuration used in our setup, can be seen as quadripolar representation as shown in Fig. 2.

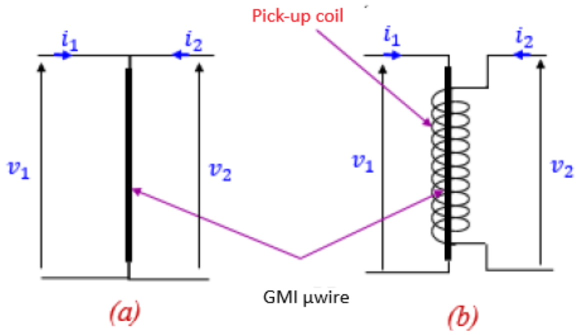


**Fig. 1.** (a) Classic GMI structure, (b) GMI wire used in off-diagonal configuration.

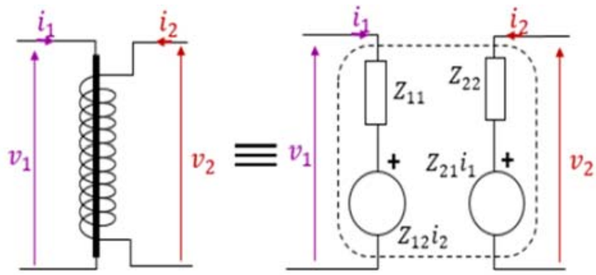


**Fig. 2.** Quadripolar representation of the wire in off-diagonal configuration.

The GMI structure can be modelled as an impedance matrix according to [10]:

$$\begin{pmatrix} v_1 \\ v_2 \end{pmatrix} = \begin{pmatrix} Z_{11} & Z_{12} \\ Z_{21} & Z_{22} \end{pmatrix} \begin{pmatrix} i_1 \\ i_2 \end{pmatrix} \quad (1)$$

where v, i are the voltage and current matrices of the quadrupole, respectively.

The impedance matrix from equation (1) shows four terms corresponding to different modes of excitation and detection:

- $Z_{11}$: µfil excited by current, with the output taken across the wire itself.
- $Z_{21}$: µfil excited by current, with the output taken across the detection coil.
- $Z_{12}$: Coil excited by current, with the output taken across the µfil.
- $Z_{22}$: Coil excited by current, with the output taken across the coil itself.

The impedances of the quadrupole in the off-diagonal GMI configuration, can be expressed in terms of the magnetic mode impedance $Z_M$ and the non-magnetic mode impedance $Z_N$ as follows [11]:

$$Z_{11} = \frac{l}{2\pi a}(Z_M cos^2\theta_M + Z_N sin^2\theta_M) \quad (2)$$

$$Z_{21} = Z_{12} = N(Z_N - Z_M) sin\theta_M cos\theta_M \quad (3)$$

$$Z_{22} = \frac{2\pi a N^2}{l}(Z_M sin^2\theta_M + Z_N cos^2\theta_M) \quad (4)$$

with $\theta_M$ designates the equilibrium position of the magnetization, a is the radius of the micro-wire, N the number of turns of the pick-up coil.

Recently, several studies show that the off-diagonal component $Z_{12}$= $Z_{21}$ is significantly more advantageous compare to the other impedance because it reduces the contribution of white noise [10, 12, 13]. Therefore, it is more beneficial to use this structure (where the wire is excited by current, and the voltage across the coil is detected) in the implementation of GMI sensors [14-15].

## 3. Theoretical Model of Temperature Sensitivity

The temperature sensitivity $S_{T21}$ of the GMI wire in off-diagonal configuration, expressed in Ω/K, indicates the variation of its impedance as a function of temperature. It is given by:

$$S_{T21} = \frac{dZ_{21}}{dT} \quad (5)$$

From equation (3), the impedance of the wire in off-diagonal mode is expressed, as a function of all the wire's parameters, such as the applied field *B*, the bias current $I_{dc}$, the magnetization and magnetic anisotropy angles $\theta_M$ and $\theta_k$, the excitation frequency $f_{ac}$, the temperature *T*, and the resistivity $\rho(T)$, according to [5]:

$$Z_{21} = \frac{N}{2} sin(2\theta_M)\left[\frac{2}{a}\rho(T) + \frac{j}{2}\mu_0 a\pi f_{ac} - (1+j)\mu_0 M_s(T)\sqrt{\frac{\pi f_{ac}\rho(T)}{\alpha_{int}(\theta_M,\theta_k) + \beta_{int}(B, I_{dc}, \theta_M, T)}}\right] \quad (6)$$

where $\mu_0$ is the permeability of free space, $\alpha_{int}$ and $\beta_{int}$ are temperature-dependent functions such that:

$$\alpha_{int} = 2k_u \cos\big(2(\theta_k - \theta_M)\big) \quad (7)$$

$$\beta_{int} = \mu_0 M_s(T)\big[H_z(B)\cos\theta_M + H_\varphi(I_{dc})\sin\theta_M\big] \quad (8)$$

Temperature also affects the magnetization angle; this implies that in the calculation of the partial derivative of impedance, the partial derivative of the magnetization angle with respect to temperature must be considered. Knowing the parameters on which the impedance depends, we can establish equation (9), assuming that the quantities $f_{ac}$, $I_{dc}$, and $\theta_k$ are constant.

$$dZ_{21}[B, I_{dc}, f_{ac}, \theta_M, \theta_k, T] = \frac{\partial Z_{21}}{\partial T}dT + \frac{\partial Z_{21}}{\partial \theta_M}d\theta_M + \frac{\partial Z_{21}}{\partial B}dB \quad (9)$$

Since the applied magnetic field is independent of the ambient temperature, the term $\frac{dB}{dT} = 0$ ; thus, the temperature sensitivity becomes:

$$S_{T21} = \frac{dZ_{21}}{dT} = \frac{\partial Z_{21}}{\partial T} + \frac{\partial Z_{21}}{\partial \theta_M}\frac{\partial \theta_M}{\partial T} \quad (10)$$

By considering the partial variations of $Z_{21}$ with respect to $\theta_M$, and expressing the variations of $\theta_M$ as a function of T, the expression for the temperature sensitivity of the off-diagonal MIG is established as follows [5]:

$$S_{T21} = \frac{N}{6a}\cos 2\theta_M[B,T]\left[12\rho[T] + ja\mu_0 f_{ac}\left(3a\pi - 2(1-j)M_s[T]\sqrt{\frac{3\pi\rho[T]}{f_{ac}k_u}}\right)\right] \times - (1+j)\frac{N}{2}\sin 2\theta_M \times \left\{\sqrt{\frac{\pi f_{ac}\rho[T]}{\alpha_{int}+\beta_{int}}}\mu_0 M'_s[T] - (1-j)\frac{\rho'[T]}{a} + \sqrt{\frac{\pi f_{ac}}{\rho[T]}}\mu_0 M_s[T]\left(\frac{(\alpha_{int}+\beta_{int})\rho'[T] - \rho[T]\frac{\partial\beta}{\partial}}{(\alpha_{int}+\beta_{int})^{3/2}}\right.\right. \quad (11)$$

The off-diagonal component and temperature sensitivity, according to equations (6) and (11), were then simulated. The simulation parameters correspond to the used microwire from Unitika Ltd. The characteristics are summarized in the Table 1. Fig. 3 shows the dependance of the off-diagonal component in function of the temperature.

Fig. 4 shows the dependance of the temperature sensitivity for different bias field.

Obtained results show that the temperature sensitivity also depends on the chosen bias point, and its variation is influenced by the sign of the applied bias field. For the used GMI wire, this variation is almost linear between -10 and 10 µT. We also note that for a zero bias field, the sensitivity is nearly zero (≈20 nΩ/°C); in other words, at this point, the sensor is insensitive to temperature. This is an interesting observation, indicating that when the bias is properly selected (*Bp* = 0), the sensor may no longer be affected by temperature. Moreover, the uniqueness of this point lies in the fact that, in the case of the off-diagonal configuration, it offers better field sensitivity and a lower noise level [10, 13, 14].

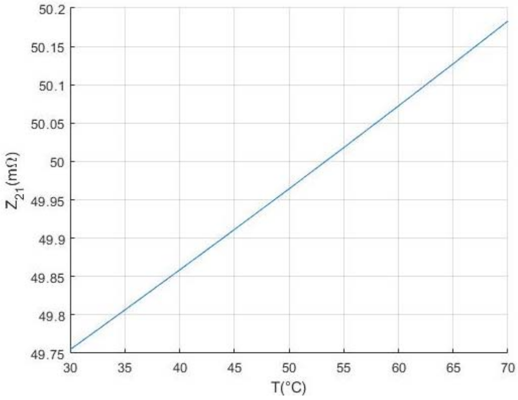


**Fig. 3.** Evolution of the MIG Impedance (mΩ) as a Function of Temperature (°C).

**Table 1.** List of parameters used in our simulation.

| Data | Value |
|---|---|
| Wire diameter, (d=2a) | $100\ \mu m$ |
| Length of the wire, (l) | $24\ mm$ |
| Number of turn ($\mathcal{N}$) | 340 |
| Anysotropy angle θk | 85° |
| DC bias current Idc | $5\ mA$ |
| Static Circumferential Field Hφ (A/m ) | $Idc/\pi d$ |
| Curie Temperature, Tc | $673\ K$ |
| $\alpha$ | $0.238\ n\Omega/mK$ |
| $\beta$ | $1.52\ \mu\Omega/m$ |
| Résistivy ρ(Ω/m) | $238.10^{-12}\,T + 1{,}52.10^{-6}$ |
| Anisotropy Constant ku | 5.636 |
| Saturation Magnetization Ms(kA/m) | $191.43(1-e^{(T-Tc)/97})$ |
| Champ axial Hz(A/m ) | $Hz=B/\mu_0$ |

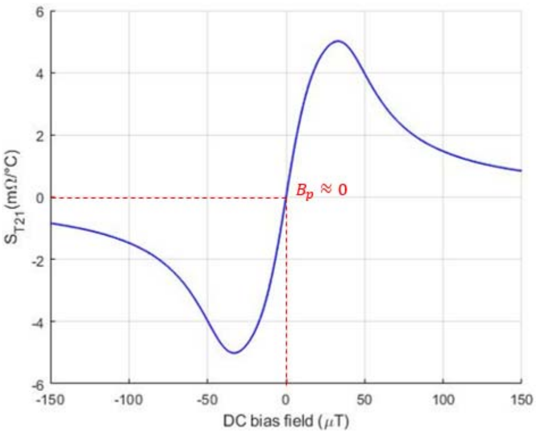


**Fig. 4.** Variation of the Temperature Sensitivity of the Wire for Different Operating Points in the Magnetic Field.

## 4. Measurement Setup

To validate our theoretical model, simulations were performed using the digital off-diagonal GMI sensor described in our recent work [13-16]. Fig. 5 illustrates the digital GMI sensor implemented in [2]. In this setup, the FPGA (Field Programmable Gate Array) circuit is situated beneath the heat sink. The wire excitation ($I_{ac}$ and $I_{dc}$) is provided by a digital frequency synthesizer (DDS, or Direct Digital Synthesizer). When an external magnetic field is applied to the sensing element in off-diagonal configuration, the voltage across the pick-up coil is amplitude-modulated by the measured field. This voltage is then transmitted to the board via the digital receiver input (SDR, or Software Defined Radio) for a quadrature digital demodulation. Both the excitation system and the digital receiver functionalities are implemented in software within the FPGA [14, 17].

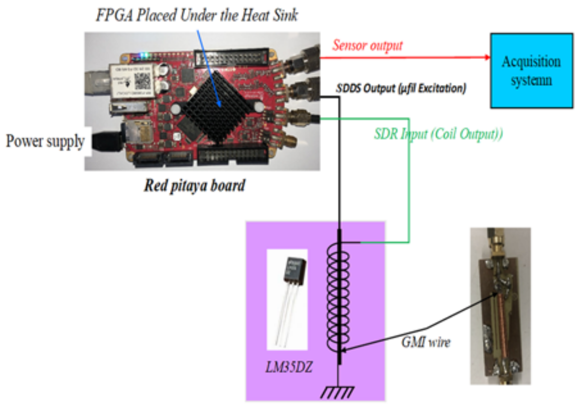


**Fig. 5.** Wiring around the FPGA Red Pitaya Development Board for Temperature Sensitivity Measurement.

The demodulated output signal is then digitized using a 16-bit data acquisition system to monitor the sensor's response to temperature variations. Measurements are conducted in a non-shielded environment. The GMI element in the off-diagonal configuration and a temperature sensor (LM35 DZ), which is used to monitor the ambient temperature, are housed within a box covered with aluminum foil. Hot air is blown into this box to create controlled temperature conditions.

To better evaluate the temperature sensitivity of the sensor, initial measurements were performed by heating the sensitive element and observing the sensor's output. Fig. 6 shows the behavior of the sensor's output over time when the GMI wire is subjected to different temperatures. This measurement was obtained under a polarization field of 10 µT.

The experimental results demonstrate the temperature sensitivity of the GMI-based sensor. In fact, when the temperature remains constant, the sensor's output is stable, indicating good reliability under steady thermal conditions.

As the temperature rises, the sensor's output increases. This behavior is attributed to changes in the magnetic and electrical properties of the GMI wire, such as magnetic permeability and impedance, which are temperature-dependent. When the heating stops, the sensor's output decreases along with the temperature, demonstrating a reversible relationship between temperature and output signal.

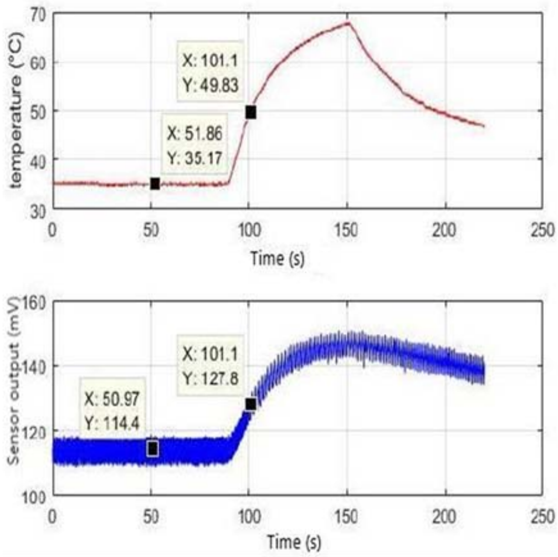


**Fig. 6.** Behavior of the offdiagonal GMI sensor output in function of the temperature for a bias magnetic fielf of 10 µT.

These results highlight the sensor's high sensitivity to temperature changes. This sensitivity can be advantageous for thermal monitoring applications but may require compensation in scenarios where temperature stability is crucial for magnetic field measurements.

To validate our theoretical approach, a measurement campaign was then conducted, followed by a statistical analysis to bound the results. To compare data under identical acquisition conditions, error bars were utilized. These graphical representations of variability illustrate whether differences between results are statistically significant. The error bars, most commonly associated with standard deviations, standard errors, or confidence intervals, provide an indication of the accuracy or uncertainty of the presented measurements.

For this study, a 95 % confidence interval (CI) was used to estimate the true value based on random sampling. The CI ensures that 95% of the observed means lie within approximately $\pm 2\sigma/\sqrt{N}$, where σ is the standard deviation, and N is the number of measurements. This statistical approach also determined the minimum number of samples required to achieve reliable results at this confidence level. Fig. 7 shows the measurement temperature sensitivity as a function of the bias magnetic field.

Fig. 8 shows an overlay of the measurement results with those from the theoretical model developed according to Equation (11).

This overlap of experimental and practical results confirms the theoretical model. Indeed, the practical results show a sensitivity profile that matches the one traced from the mathematical model within the dynamic range. Furthermore, at the zero bias point, the observation made in the simulation is confirmed by the measurements, with a sensitivity much lower than at other points, approximately -0.2 mΩ/°C. Similarly, the linearity observed around zero is also reflected in practice.

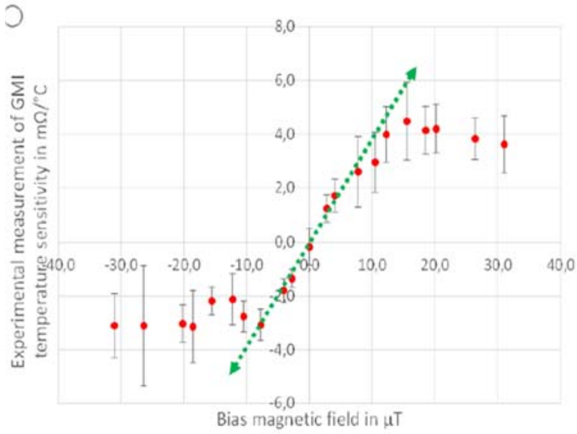


**Fig. 7.** Experimental behaviour of GMI Temperature sensitivity in mΩ/°C versus DC bias magnetic field in µT.

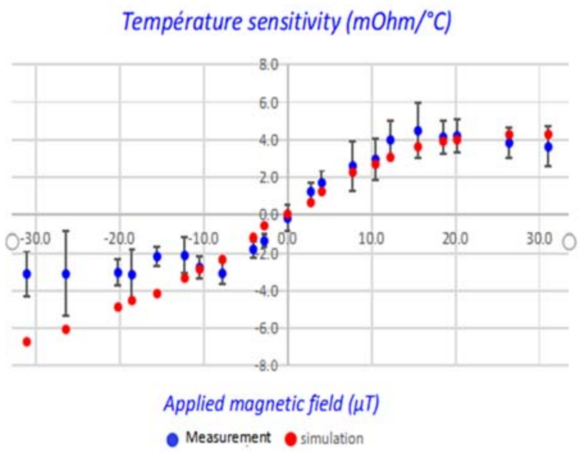


**Fig. 8.** Overlay of experimental and theoretical Results.

In summary, a good agreement is observed, especially for positive fields and fields around zero, with theoretical values falling within the established confidence intervals. However, a significant discrepancy is noted between -10 and -31 µT.

The observed difference between theory and practice can primarily be attributed to the theoretical parameters used in our simulation, such as the magnetic anisotropy field, the saturation magnetization, and the magnetic anisotropy angle. To better understand the impact of each parameter, several simulations were conducted. Fig. 9 shows the behavior of temperature sensitivity for different values of the magnetic anisotropy field.

A discrepancy is observed starting from −20 µT towards the more negative fields. When its magnitude decreases from 46 to 34 A/m, the sensitivity curve rises starting from −20 µT. An interesting observation, since in Fig. 8, a similar discrepancy between the theoretical and practical curves is noted starting from −10 μT.

In the state of the art, the saturation magnetization values are typically on the order of a few hundred kA/m. We have again simulated the temperature sensitivity by first multiplying it by 2, then by 0.8. Fig. 10 shows the obtained results.

We observe that the saturation magnetization has a slight influence on the shape of the sensitivity curve. When it decreases from 191430 to 153144 A/m, its influence remains negligible, as practically its value is on the order of 190000 A/m.

Fig. 11 shows the theoretical temperature sentivity curves for different value of anisotropy angle.

The variation of the anisotropy angle, like the anisotropy field, does have an influence on the sensitivity. When it changes from −85 to 90° C, the sensitivity curve rises starting from −10 μT and is slightly lowered from 10 μT onwards. These observations are similar to the experimental curve obtained.

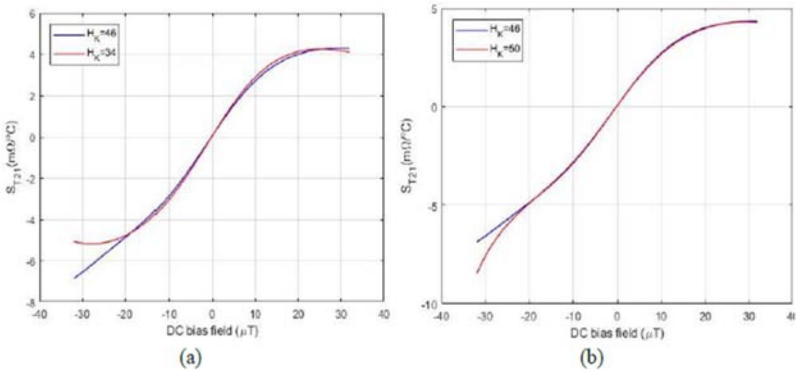


**Fig. 9.** Theoretical temperature sensitivity curves for an anisotropy of 46 A/m (used previously). (a) In red, a new anisotropy value of 34 A/m; (b) In red, a new anisotropy value of 50 A/m.

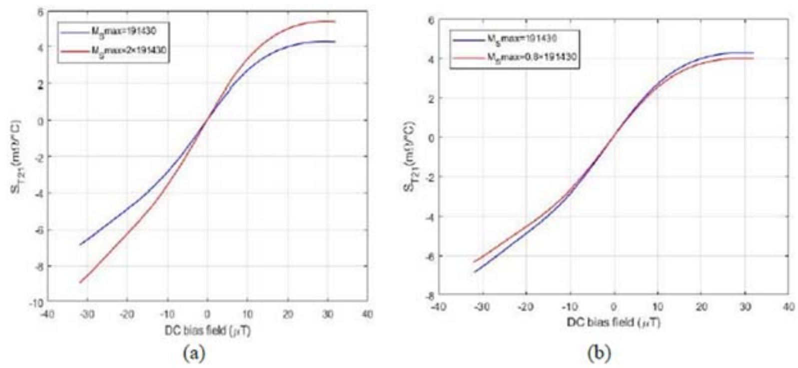


**Fig. 10.** Theoretical sensitivity curves with respect to temperature for a maximum saturation magnetization of 191430 A/m (used previously). In red, an amplitude of 2*191430 A/m; (b) In red, an amplitude of 0.8*191430 A/m.

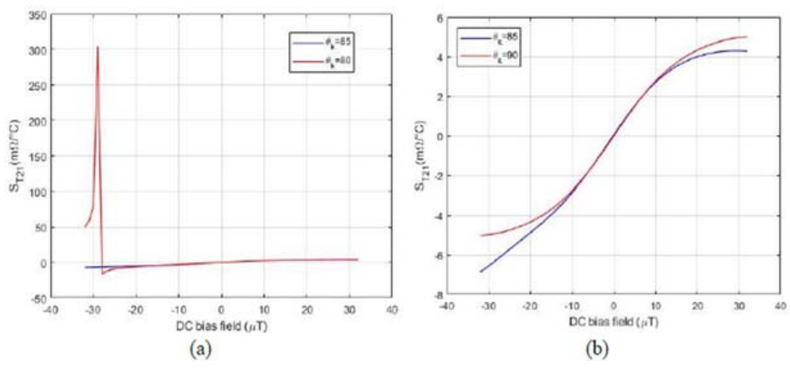


**Fig. 11.** Theoretical temperature sensitivity curves for an anisotropy angle of 85° (used previously). (a) In red, the angle is 80°; (b) In red, the angle is 90°.

The analysis of the modification of these intrinsic parameters in the GMI wire shows that the quantities whose variation has the most influence on the agreement between the theoretical and practical curves are the magnetic anisotropy field and the magnetization angle. In fact, magnetic anisotropy (both magnitude and direction) results from the tendency of spin moments to align along an easy magnetization direction rather than a hard magnetization direction. This anisotropy is typically linked to the crystalline structure or shape of the material. It arises from interactions between the electronic spins and the crystal field of the material, as well as from demagnetizing fields (shape anisotropy).

In the case of amorphous wires, the magnetic anisotropy that remains is largely due to mechanical stresses introduced during the rapid solidification process during manufacturing. These stresses typically result in a constant anisotropy field. However, this anisotropy field can change when the wire is subjected to additional mechanical stress.

During the fabrication of the sensing element (comprising the wire and detection coil), the wire was in contact with metallic tools such as soldering irons and cutting pliers, which bent or heated the wire. These processes altered the previously defined anisotropy properties established by the manufacturer, thereby introducing slight variations in the magnetic characteristics of the wire. These variations are likely responsible for the small discrepancy observed between the theoretical simulations and the experimental measurements.

## 5. Conclusion

This article provides a comprehensive analysis of the temperature sensitivity of a digital GMI (Giant Magnetoimpedance) sensor by comparing experimental results with theoretical predictions. The experimental data demonstrate a strong alignment with the theoretical model, particularly within the dynamic range studied. This consistency validates the robustness of the model, confirming that it accurately predicts the sensor's behavior under varying conditions.

At the zero bias point, the measured sensitivity is significantly lower than at other points, which aligns well with the theoretical predictions, where the sensitivity is approximately -0.2 mΩ/°C. This result is particularly important as it supports the validity of the theoretical approach, highlighting the precise control of temperature sensitivity around this critical point. Furthermore, the linearity observed around the zero bias point is also in excellent agreement with theoretical expectations, further confirming the accuracy of the model.

The agreement between experimental and theoretical results is notably strong for positive magnetic fields and those near zero, where the theoretical values fall within the established confidence intervals. This consistency suggests that the model accurately captures the key physical phenomena governing the sensor's performance in these regions. However, a notable discrepancy was observed in the range of -10 to -31 μT, where the experimental data deviated from the theoretical predictions. This discrepancy points to areas where the model may require refinement or where additional factors—such as material imperfections or measurement errors—may be influencing the results.

These findings not only validate the strength and reliability of the theoretical model but also reveal areas for potential improvement. Ultimately, the results of this study pave the way for further developments in the field, offering valuable insights that can contribute to enhancing the accuracy and reliability of GMI sensors in practical applications, particularly in fields such as medical devices, industrial sensing, and environmental monitoring.

## References


[1]. K. V. Rao, F. B. Humphrey, J. L. Costa-Kramer, Very large magnetoimpedance in amorphous soft ferromagnetic wires, *Journal of Applied Physics*, Vol. 76, Issue 10, 1994, pp. 6204-6208.

[2]. L. Panina, K. Mohri, Magneto-impedance effect in amorphous wires, *Applied Physics Letters*, Vol. 65, 1994, pp. 1189-1191.

[3]. E. P. Harrison, G. L. Turney, H. Rowe, Electrical properties of wires of high permeability, *Nature*, Vol. 135, Issue 3423, 1935, pp. 961.

[4]. P. Ripka, Magnetic Sensors and Magnetometers, *Artech House Publisher*, 2001.

[5]. A. Esper, B. Dufay, S. Saez, C. Dolabdjian, Theoretical and Experimental Investigation of Temperature-Compensated Off-Diagonal GMI Magnetometer and Its Long-Term Stability, *IEEE Sensors Journal*, 20, 16, 2020, pp. 9046-9055.

[6]. L. Kraus, M. Malatek, M. Dvorak, Magnetic field sensor based on asymmetric inverse Wiedemann effect, *Sensors and Actuators A: Physical*, Vol. 142, Issue 2, 2008, pp. 468-473.

[7]. A. S. Antonov, I. T. Iakubov, A. N. Lagarkov, Longitudinal-transverse linear transformation of the HF-current in soft magnetic materials with induced anisotropy, *IEEE Transactions on Magnetics*, Vol. 33, Issue 5, 1997, pp. 3367-3369.

[8]. S. Sandacci, D. Makhnovskiy, L. Panina, K. Mohri, Y. Honkura, Off-diagonal impedance in amorphous wires and its application to linear magnetic sensors, *IEEE Transactions on Magnetics*, Vol. 40, Issue 6, Nov. 2004, pp. 3505–3511.

[9]. E. Paperno, Suppression of magnetic noise in the fundamental-mode orthogonal fluxgate, *Sensors and Actuators A: Physical*, Vol. 116, Issue 3, October 2004, pp. 405–409.

[10]. B. Dufay, S. Saez, C. P. Dolabdjian, A. Yelon, D. Ménard, Characterization of an optimized Off diagonal GMI-based Magnetometer, *IEEE Sensor Journal*, Vol. 13, Issue 1, January 2013, pp. 379-388.

[11]. L. Ding, Étude et amélioration des performances en bruit de capteurs à MagnétoImpédance Géante: Application à la magnétométrie à très haute sensibilité, Thèse de Doctorat en Électronique et

Microélectronique, *Université de Caen*, 2008 (in French).

[12]. M. Malatek, B. Dufay, S. Saez, C. Dolabdjian, Improvement of the off-diagonal magnetoimpedance sensor white noise, *Sensors and Actuators A: Physical*, Vol. 204, December 2013, pp. 20–24.

[13]. P. S. Traoré, A. Asfour, J. P. Yonnet, C. Dolabdjan, Noise Performance of SDR-Based Off-Diagonal GMI Sensors, *IEEE Sensors Journal*, Vol. 17, Issue 19, October 2017, pp. 6175-6184.

[14]. P. S. Traoré, A. Asfour, J. P. Yonnet, Design Approach for an Off-Diagonal Giant Magneto Impedance Sensor Based on Field Programmable Gate Array, *Sensors and Transducers*, Vol. 245, Issue 6, October 2020, pp. 20-26.

[15]. P. S. Traoré, S. Konan, A. Asfour, J. P. Yonnet, Analysis of the impact of the processing time-delay on the stability of a digital GMI magnetometer, in *Proceedings of the IEEE Sensors Conference*, 31 October 4 November 2021, pp. 1-4.

[16]. P. S. Traoré, A. Asfour, S. Konan and J. -P. Yonnet , Stability Criteria of a High Sensitivity Digital GMI Magnetometer, *IEEE Transactions on Magnetics*, Vol. 59, Issue 2, February 2023, 6100204.

[17]. P. S. Traoré, A. Asfour, J.-P. Yonnet, C. Boudinet, Introduction of real-time digital processing techniques for the high-sensitivity GMI sensors, *International Journal of Applied Electromagnetics and Mechanics*, Vol. 59, Issue 2, 2019, pp. 455-463.